Renewable and Sustainable Energy Reviews 47 (2015) 416–426

Contents lists available at ScienceDirect

Renewable and Sustainable Energy Reviews

journal homepage: www.elsevier.com/locate/rser

Modelling and sensitivity analysis of isolated microgrids

A.M. Abd-el-Motaleb *, Dean Hamilton

Department of Electrical Engineering, University of Warwick, Coventry CV4 7AL, United Kingdom

ARTICLE INFO

Article history:
Received 12 September 2014
Received in revised form
2 January 2015
Accepted 8 March 2015
Available online 30 March 2015

Keywords:
Microgrids
Small-signal stability
Distributed generation
Doubly fed induction generator

ABSTRACT

In conventional generation systems, the possibility of system restoration and reducing power swings among different generation units is high, as an adequate reserve can be supplied from neighboring generation units to restore the operation. In contrast, the situation is different in the case of isolated microgrids, as the system reserve and capabilities of the whole system to recover from disturbances are limited, especially when the microgrid is supplied by intermittent sources as wind energy. This paper presents the state space modelling of isolated microgrids supplied by different energy sources, and thereafter, the eigenvalue sensitivity analyses are conducted. The main contribution of this paper is that a detailed model of an isolated microgrid supplied by different energy sources, particularly battery units and doubly-fed induction generators is presented. Moreover, in contrast to the most recent papers, which have discussed the state space modelling of several energy sources and have not studied the effect of load dynamics on the stability of power systems, this paper includes the dynamics of two of the most common loads, heating and induction machines. Their effects on the stability of the microgrid are discussed in detail.

© 2015 Elsevier Ltd. All rights reserved.

Contents

1. Introduction

Traditionally, the question of power system stability has been connected to maintaining synchronism among energy sources. The production of electricity in the conventional utility is primarily

* Corresponding author.
E-mail address: A.Motalab@warwick.ac.uk (A.M. Abd-el-Motaleb).

http://dx.doi.org/10.1016/j.rser.2015.03.025
1364-0321/© 2015 Elsevier Ltd. All rights reserved.

Nomenclature

A, B, C, D	state variables, control, output, and feed-forward matrices, respectively
P_{max}	inverter maximum power
C	battery stored energy
Δt	time interval
$P_t^{E_d}$, $P_t^{E_c}$	battery discharge/charge power
η_d, η_c	battery discharge/charge efficiency
m_p	inverter droop coefficient
κ	battery charging level
δ	coordinate angle of rotation
i_i, i_o	LCL filter input/output currents
v_o, v_g	LCL capacitor voltage and microgrid node voltage, respectively
ω	grid operating frequency
$\tilde{p}$, $\tilde{q}$	inverter instantaneous active and reactive power, respectively
ω_c	cut-off frequency
P, Q	active and reactive power, respectively
Δ	linearized variables operator
T_e, T_{sh}	wind turbine electrical and shaft torque, respectively
H_t, H_g	turbine and generator inertia constants, respectively
θ_{tw}	wind turbine shaft twist angle
ω_t, ω_r	wind turbine and generator angular speeds, respectively
ω_s, ω_{elb}	wind turbine synchronous and electrical base speeds, respectively
K_{sh}	wind turbine shaft stiffness
V_{dc}	dc-link voltage
z_P	thermostatic load state variable
α_t	transient load exponent
T_P	thermostatic load time constant
H	induction machine inertia constant
T_m, T_{e_m}	induction machine mechanical and electrical torque, respectively
s	induction machine slip
T_2	induction machine constant
d	subscript denoting the direct-axis component of a variable
q	subscript denoting the quadrature-axis component of a variable
$*$	superscript denoting a reference value
$\cdot$	superscript denoting differentiation with respect to time

secured using synchronous generators, and for that reason it is important to secure their synchronism and parallel operation. Therefore, the question of stability in conventional power systems is mainly based on the stability of synchronous machinery and on the relationship between the active power and rotor angle of the generator [1,2].

Nowadays, the justification for the large centralized station has weakened due to depleting conventional resources, increased transmission and distribution costs, deregulation trends and environmental concerns. Distributed generation sources (DGs) are commonly used for small scale generation and can offer a solution to many of the centralized generation challenges [3,4].

Microgrids are considered as clusters of distributed energy sources, loads and controls, organized to deliver the optimum energy service [5]. The most common perturbations in power networks can be analyzed by the small signal stability study. The small signal stability analyses have been investigated in several papers. In [6,7], both Lihui and Yang, respectively, presented stability analyses of microgrids supplied by the main utility along with the contribution from wind energy to detect the critical modes, which can influence the stability. In [8], Zhixin studied the inter-area oscillation problems caused by high penetration of grid-connected doubly fed induction generators (DFIGs), and a damping controller was designed to show the competency of that controller. Amir in [9] investigated the modelling and stability analysis of DFIGs interfaced to the grid via a series-compensated transmission line, and the critical parameters, which influence the system stability, were identified. A coordinated tuning of the controller to enhance the damping of the oscillatory modes, which can deteriorate the stability of DFIGs in grid-connected mode, was shown by Yateendra in [10]. The use of energy storage systems for a grid-connected doubly fed induction generator was shown in [11] by Mishra. The storage systems were employed to counter the intermittent nature of wind turbine power. A coordinated control scheme was used to enhance the damping of the oscillatory modes.

DGs are normally located near to customers and are interfaced to networks via electronic inverters to regulate the output. DGs interfaced via inverters are considered one of the most common energy sources supplying microgrids. In [12], Zhixin conducted a small signal stability analysis of an isolated microgrid, supplied by a synchronous generator operating as a slack bus and other DGs interfaced by electronic inverters to detect the critical modes. In [13], Bottrell focused on the control loop dynamics of the converters, which interface DGs to supply isolated microgrids. The converters models were linearized and the participation analysis of the critical eigenvalues was presented for the whole microgrid. The author showed that the critical eigenvalues are mainly associated with the voltage and droop controller state variables of the converters. In [14], Hassan provided stability analysis of microgrids supplied through inverters. Optimal design of inverter control loops was implemented and the control parameters were generated by particle swarm optimization.

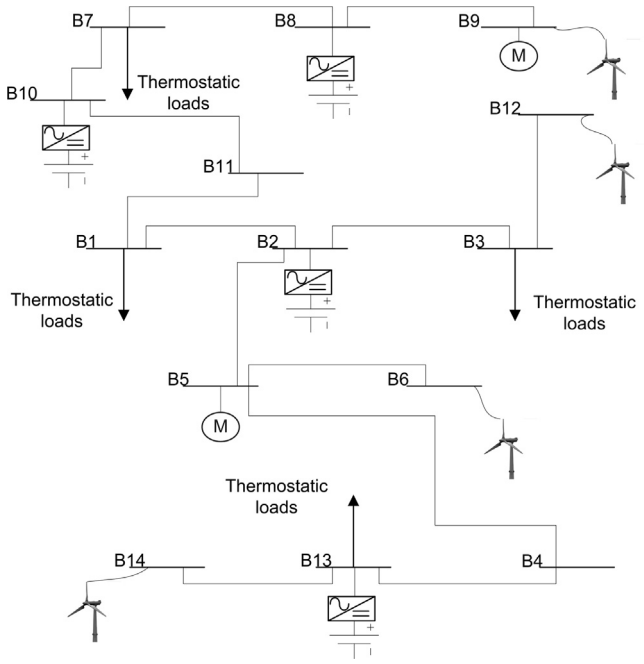

Fig. 1. Microgrid layout

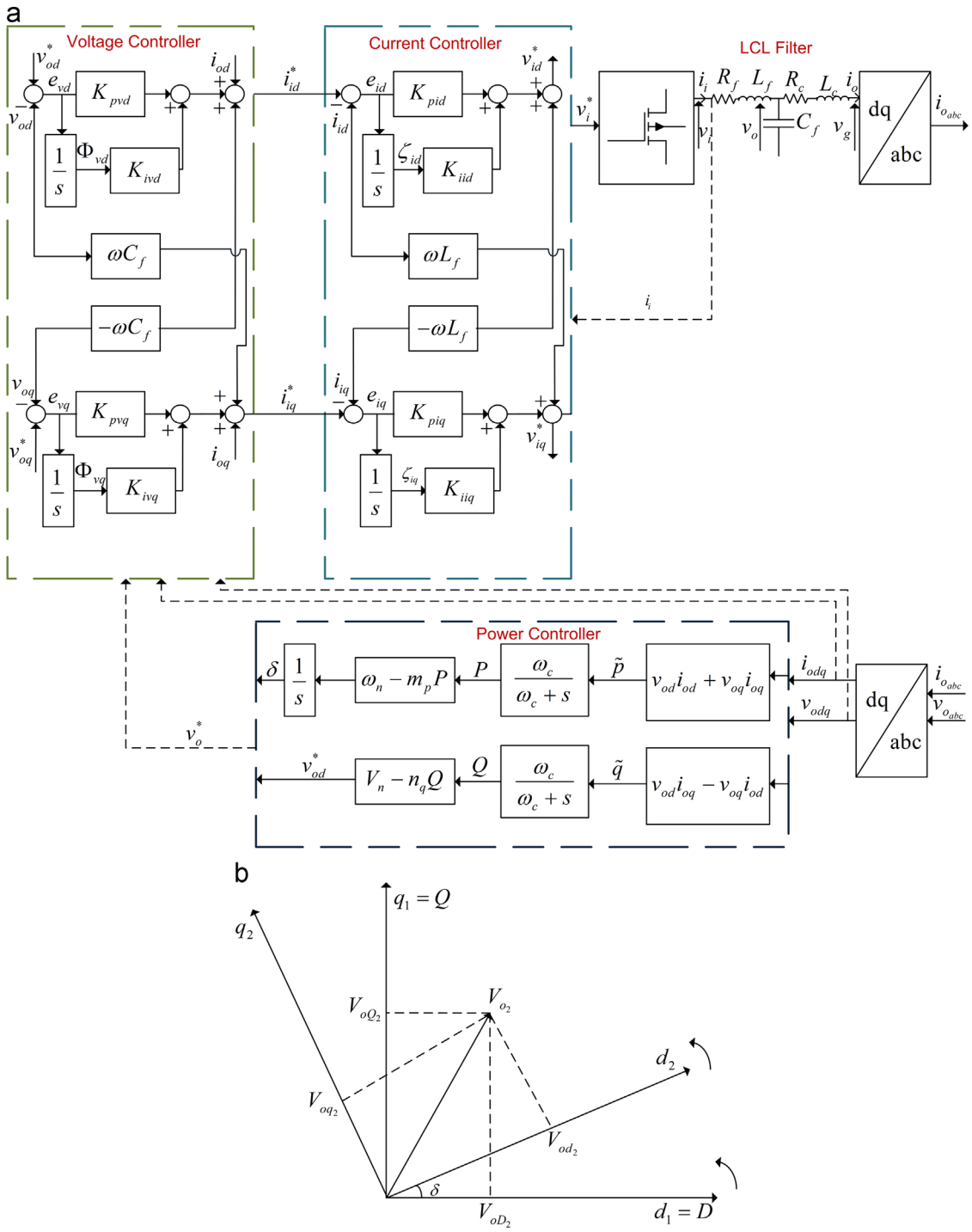

Fig. 2. Voltage–frequency inverter

The eigenvalue and time-domain analyses were shown in [12] to clarify the interaction between the diesel generator and inverter-based DGs. The stability problem of microgrids supplied by DGs interfaced via inverters was analyzed in [15]. Stability degradation was referred to the droop controllers of the inverters, and subsequently a coordinated optimization of the droop coefficients was processed based on matrix perturbation theory.

All the previous power system stability studies belong to either power networks supplied by wind generators and connected to utility grids, or to isolated networks supplied by dispatchable distributed generators interfaced by electronic inverters and without any penetrations of intermittent energy sources. Moreover, the load dynamics were not considered through the previous articles as contributing factors to bifurcations. Therefore, a clear idea concerning the *practical* instability and bifurcation events has not been fully explained.

However, in rural areas, it is very difficult as well as uneconomical to transmit power over long distances through transmission lines to supply such areas. Isolated microgrids, which are dependent on renewable sources, provide a promising alternative means to satisfy the energy requirements for those areas. When integrating intermittent energy sources such as wind to the network, additional capacity is needed to meet actual load demand. The characteristics of such grids require scheduling more reserve for

ensuring adequate security and reliability levels. Thereby, storage systems are often required along with renewable sources to supply such grids.

In this paper, a detailed dynamic model of a microgrid supplied from DFIGs and energy storage systems is proposed. The proposed microgrid supplies two types of the most common loads, heating and induction machine loads. The induction machine is modelled as quadratic torque induction motor, and the heating loads are modelled as groups of thermostatic loads and represented by multiplicative generic load models.

The main purpose of this paper is to study the stability of an isolated mirogrid characterized by limited power capability as it is supplied from battery units limited by the charging level, and intermittent energy source (DFIGs), along with the contribution of load dynamics. Another purpose is to focus on the oscillatory instability, which results from perturbations of specific parameters as will be shown in Section 4.#

2. Microgrid layout

Fig. 1 shows the layout of the proposed isolated microgrid. The base power of the microgrid is 1 MW, and the microgrid consists of a 14 node distribution system, thermostatic loads represented by multiplicative generic models, and two groups of quadratic torque induction machines. The network includes two types of energy sources; the first is non-dispatchable, DFIGs, and the second is dispatchable, battery units. Each DFIG is rated at 1.5 p.u. whereas each DG is rated at 0.8 p.u. The thermostatic loads add up to 0.6 p.u. and the groups of quadratic torque induction machines add up to 1.8 p.u.

For brevity, it is assumed that the reader is already familiar with the basic concepts of power system modelling. Thus, the state space models of thermostatic loads, quadratic torque induction machines and distribution lines will not be covered in this paper, and the focus will be directed towards the modelling of the distributed energy sources.#

3. Microgrid state space modelling

The microgrid state variables are chosen based on the microgrid elements, which are capable of storing energy. These elements include inductive, capacitive and integrator elements [16], which are included in the proposed microgrid plant model to be controlled. Thereafter, the microgrid dominant eigenvalues can be detected. The final linearization form can be described by

$$\Delta\dot{x}(t) = A\Delta x(t) + B\Delta u(t) \tag{1}$$

$$\Delta y(t) = C\Delta x(t) + D\Delta u(t) \tag{2}$$

3.1. Voltage–frequency inverter

Typically, the batteries are rated to a certain capacity and feed droop-regulated inverters. Each inverter has a maximum power constraint,P_{max}, due to the available capacity of the batteries. The

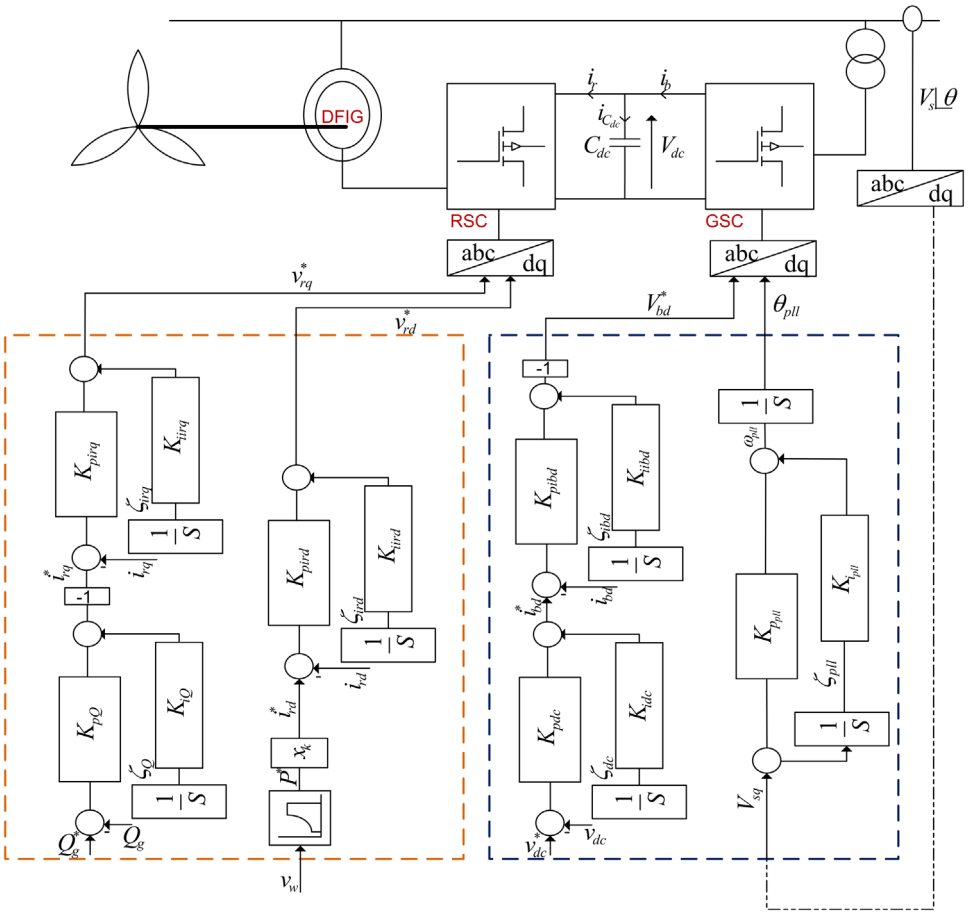

Fig. 3. DFIG control scheme

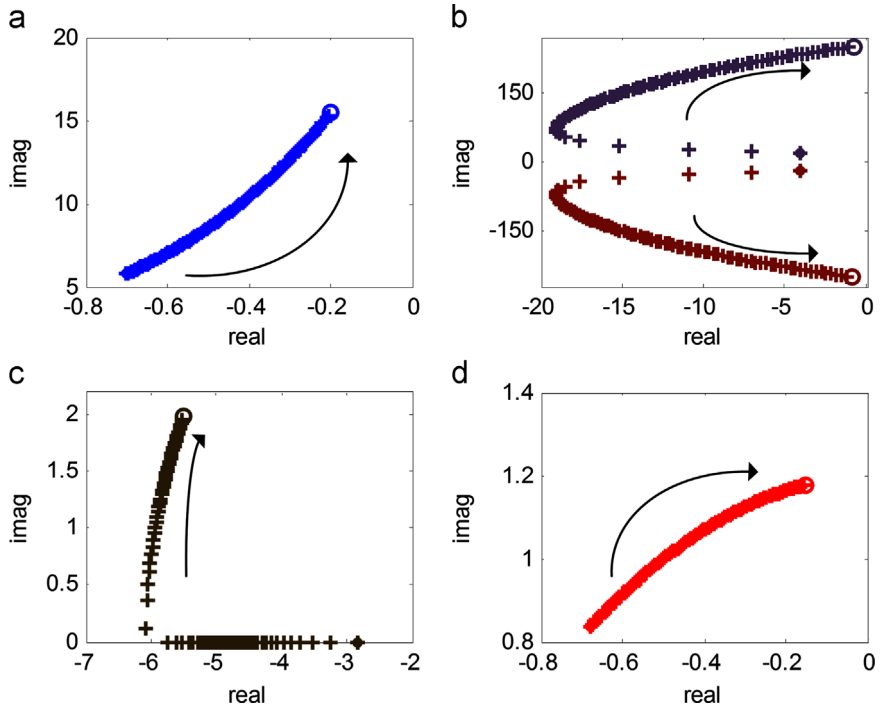

Fig. 4. Eigenvalue loci during wind speed increment (K_{pdc} and $K_{idc}=1.1$) of modes affected by (a) turbine speed and shaft twist angle, (b) magnetization current, (c) coordinates' angles of rotation, and (d) dc-link voltage.

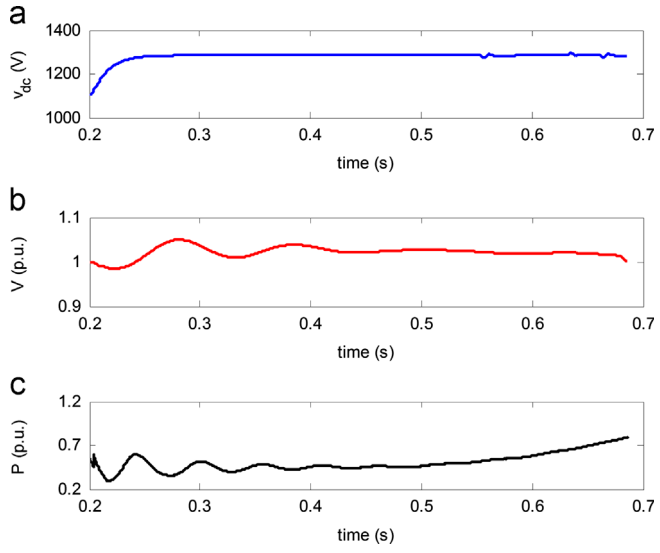

Fig. 5. Simulation results during stable mode of operation: (a) dc-link voltage, (b) voltage at B9, and (c) DFIG power at B9.

charging–discharging battery process is based on [17] and is shown in

$$\text{Disch}: \quad C(t+1)=C(t)-\Delta t\frac{P_t^{E_d}}{\eta_d}$$

$$\text{Ch}: \quad C(t+1)=C(t)+\Delta t\times(P_t^{E_c}\times\eta_c). \tag{3}$$

Based on [18], the modelling of voltage–frequency inverters are presented. The droop coefficients of the inverters are adjusted according to the charging level of the batteries, as per

$$m_p=\frac{m_{p_{min}}}{\kappa}$$

$$s.t.\ \ 0.01\le\kappa\le 1. \tag{4}$$

The charging levels of the battery units can be directly introduced as fixed limits. However, for computational purposes, the charging levels of the battery units are represented by adjusting the droop coefficients of the inverters, as shown in (4).

The proposed model of the voltage–frequency inverter is shown in Fig. 2(a). Fig. 2(b) shows the reference frame of the master DG, which is denoted by DQ coordinates. If another DG is decomposed into dq_2 coordinates, and is connected to the micro-grid, this energy source will be displaced from the DQ reference frame by a rotation angle δ_2.

3.1.1. LCL filter

The state variables of the LCL filter are chosen as the inductance currents i_i, i_o and the voltage across the capacitor v_o Fig. 4. The linearized model of the LCL filter is shown by

$$\begin{bmatrix}\dot{i}_{id}\\ \dot{i}_{iq}\\ \dot{v}_{od}\\ \dot{v}_{oq}\\ \dot{i}_{od}\\ \dot{i}_{oq}\end{bmatrix}=A_F\begin{bmatrix}i_{id}\\ i_{iq}\\ v_{od}\\ v_{oq}\\ i_{od}\\ i_{oq}\end{bmatrix}+B_F\begin{bmatrix}\Delta v_{id}\\ \Delta v_{iq}\\ \Delta v_{gd}\\ \Delta v_{gq}\end{bmatrix}+\begin{bmatrix}I_{iq}\\ -I_{id}\\ V_{oq}\\ -V_{od}\\ I_{oq}\\ -I_{od}\end{bmatrix}[\Delta\omega]. \tag{5}$$

$$\begin{bmatrix}\dot{i}_{id}\\ \dot{i}_{iq}\\ \dot{v}_{od}\\ \dot{v}_{oq}\\ \dot{i}_{od}\\ \dot{i}_{oq}\end{bmatrix}=A_F\begin{bmatrix}i_{id}\\ i_{iq}\\ v_{od}\\ v_{oq}\\ i_{od}\\ i_{oq}\end{bmatrix}+B_F\begin{bmatrix}\Delta v_{id}\\ \Delta v_{iq}\\ \Delta v_{gd}\\ \Delta v_{gq}\end{bmatrix}+\begin{bmatrix}I_{iq}\\ -I_{id}\\ V_{oq}\\ -V_{od}\\ I_{oq}\\ -I_{od}\end{bmatrix}[\Delta\omega]. \tag{6}$$

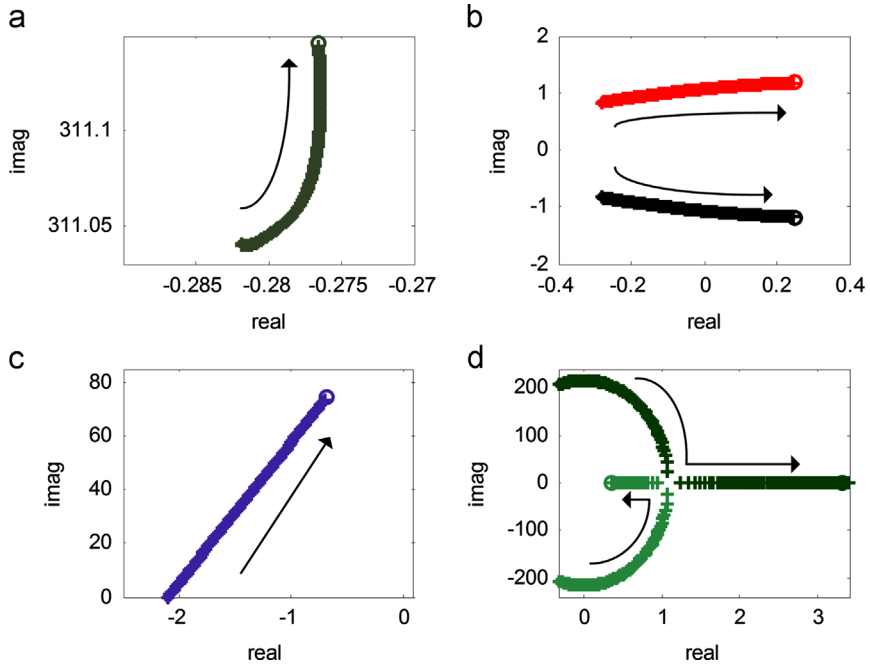

Fig. 6. Eigenvalues loci during wind speed increment (K_{pdc} and K_{idc}=0.1) of modes affected by (a) magnetization current, (b) turbine speed and shaft twist angle, (c) coordinates' angles of rotation, and (d) dc-link voltage.

$$B_F = \begin{bmatrix} \frac{1}{L_f} & 0 & 0 & 0 \\ 0 & \frac{1}{L_f} & 0 & 0 \\ 0 & 0 & 0 & 0 \\ 0 & 0 & 0 & 0 \\ 0 & 0 & \frac{-1}{L_c} & 0 \\ 0 & 0 & 0 & \frac{-1}{L_c} \end{bmatrix}. \quad (7)$$

3.1.2. Power controller

The external power control loop sets the magnitude of the frequency and inverter output voltage, according to the droop characteristics for the real and reactive power. The instantaneous active and reactive power components $\tilde{p}$ and $\tilde{q}$, respectively, are calculated from the measured output voltage and current. The instantaneous power components are passed through low-pass filters of cut-off frequency ω_c to limit the high transient variation, Fig. 2(a).

The linearized equation of the power controller is indicated by (8), where I_{od}, I_{oq}, V_{od}, and V_{oq} represent the operating point variables.

$$\begin{aligned} \Delta\dot{P} &= -\omega_c\Delta P + 1.5\omega_c(\Delta v_{od}I_{od} + \Delta v_{oq}I_{oq} + V_{od}\Delta i_{od} + V_{oq}\Delta i_{oq}) \Delta\dot{Q} \\ &= -\omega_c\Delta Q + 1.5\omega_c(\Delta v_{oq}I_{od} - \Delta v_{od}I_{oq} + V_{oq}\Delta i_{od} - V_{od}\Delta i_{oq}). \end{aligned} \quad (8)$$

3.1.3. Voltage–current controller

The voltage control is processed through PI controllers, and the inverter voltage is decomposed into dq coordinates. Moreover, the voltage across the q coordinate is assumed to be zero.

Fig. 2(a) illustrates the inverter voltage–current controller; the dynamic equations of the voltage–current controller are indicated by (9). The state variables in this case output from the controller integrators are

$$i_{id}^* - i_{id} = e_{id}\,,\; i_{iq}^* - i_{iq} = e_{iq}\,,\; v_{od}^* - v_{od} = \dot{\Phi}_{vd}\,,\; v_{oq}^* - v_{oq} = \dot{\Phi}_{vq}. \quad (9)$$

Table 1
Dominant state variables for wind speed increment scenario.

λ	Dominant states	Participation factor	Final remarks
$-0.3+j0.9$	Mechanical, θ_{tw}, ω_t	0.42	Unstable (Hopf bifurcation)
$-3+j200$	Electrical, v_{dc}	1	Unstable (Hopf bifurcation)
-2.2	Electrical, δ	0.6	Stable

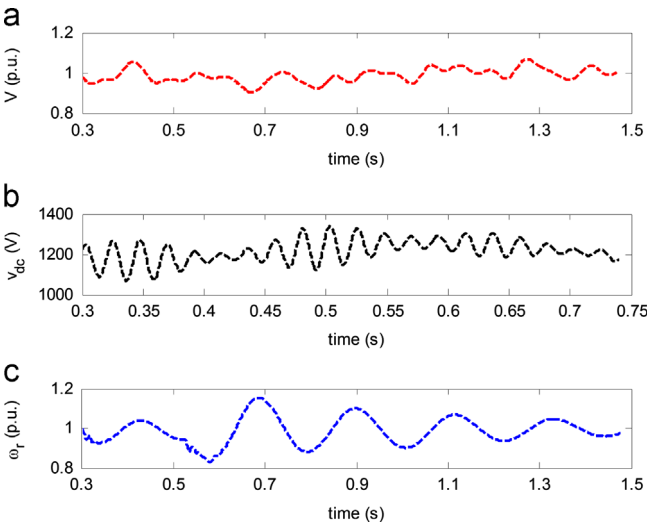

Fig. 7. Simulation results during stable mode of operation: (a) voltage at B9, (b) dc-link voltage, and (c) DFIG mechanical speed at B9.

3.2. Doubly-fed induction generator

The doubly-fed induction generator is modelled as a wound rotor induction machine of the third order. The AC/DC/AC converter is divided into the rotor side converter and grid side converter; also

there is a connected capacitor on the dc side, which acts as a dc voltage source. The rotor side converter is used to control the wind turbine output real power, whereas the grid side converter is used to regulate the voltage of the dc bus capacitor.

In [19], the electrical part of the DFIG model was considered; the drive train model was excluded. However, in [20] it was shown that the first critical oscillatory modes resulting from small signal stability analysis are associated with the drive train model of the DFIG.

Usually, it is adequate to represent the drive train by a two-mass model, assuming that the modes of the blades and hub are well damped [21]. Thereby, the proposed model of this paper combines the electrical and mechanical parts in [19,20], respectively. The detailed model of the DFIG used in this paper is shown in Fig. 3.

3.2.1. Turbine and drive train

In this model, the two-mass drive train model is adopted; the assumption is made that the blade pitch angle is constant. The dynamics are shown by the following equations:

$$2H_t\frac{d\omega_t}{dt}=T_m-T_{sh}\,,\frac{1}{\omega_{elb}}\frac{d\theta_{tw}}{dt}=\omega_t-\omega_r\,,2H_g\frac{d\omega_r}{dt}=T_{sh}-T_e. \quad (10)$$

3.2.2. Rotor-side converter

The proposed control scheme of the rotor-side converter is shown in Fig. 3. In order to decouple the electromagnetic torque and rotor excitation current, the induction generator is controlled in a synchronous rotating stator-flux-oriented reference frame, with its *d*-axis oriented along the stator-flux vector position.

The first part of the rotor-side converter controller aims at controlling the active power, so as to track the reference power P^*, Fig. 3. The reference active power is determined by the wind turbine power speed characteristic curve for maximum power extraction. The second part of the rotor-side converter controller is shown in Fig. 3, and aims at controlling the reactive power. The linearized model of the rotor-side converter is shown in the following equation:

$$\Delta\dot{\zeta}_Q=-\Delta Q_g\,,\Delta\dot{\zeta}_{i_{rd}}=\Delta i_{rd}^*-\Delta i_{rd}\,,\Delta\dot{\zeta}_{iq}=\Delta i_{rq}^*-\Delta i_{rq}. \quad (11)$$

Table 2
Dominant state variables for droop coefficients increment scenario.

λ	Dominant states	Participati-on factor	Remarks
$-0.9+j311$	Electrical,$i_{m_{dq}}$	0.127	Stable
−3	Electrical, δ	0.39	Unstable-(Hopf bifurcation)
−0.85	Electrical, v_{dc}	0.5	Stable
−1.35	Electrical, Z_P	0.4	Stable

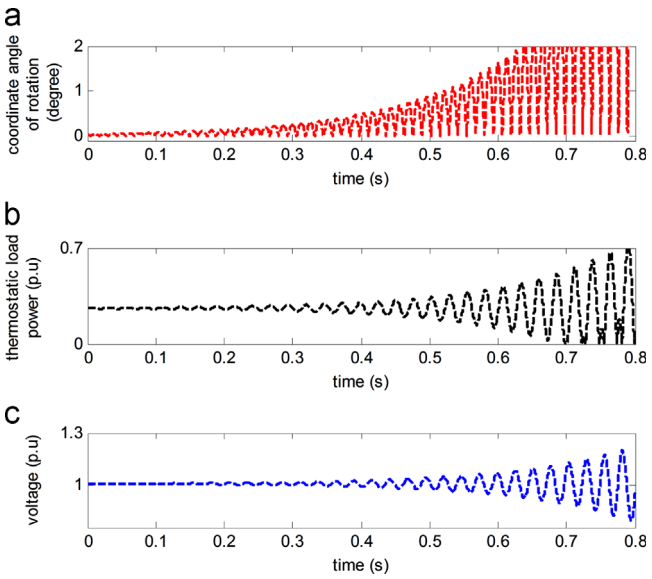

Fig. 9. Effect of inverters droop increment: (a) coordinate angle of rotation at B13, (b) thermostatic load power at B13, and (c) voltage at B13

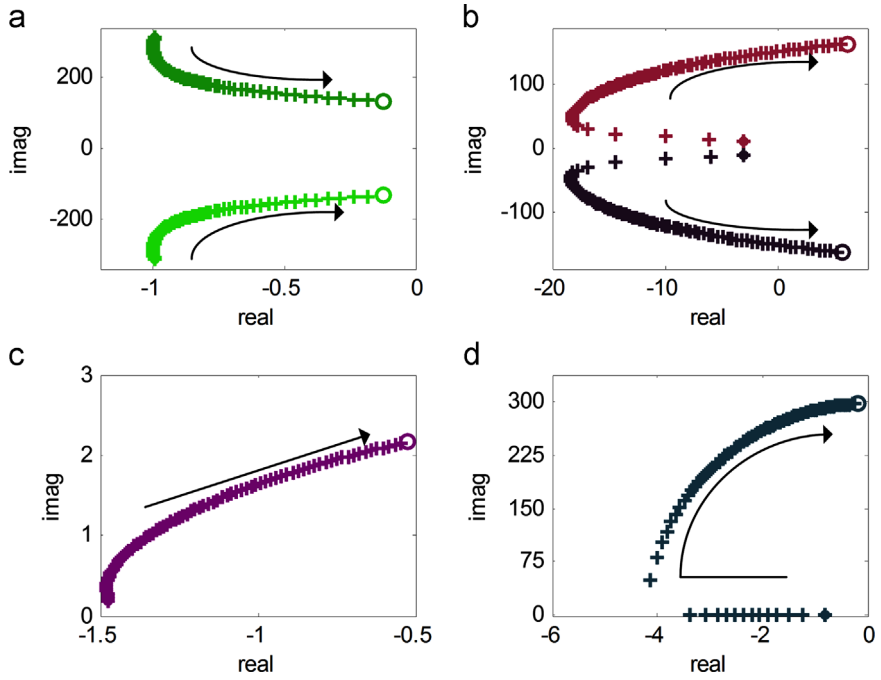

Fig. 8. Eigenvalues loci during droop coefficients increment of modes affected by (a) magnetization current, (b) coordinates' angles of rotation, (c) thermostatic load state variable, and (d) dc-link voltage.

3.2.3. DC-link circuit

The linearized energy balance of the dc-link capacitor is shown in (12). The dc-link voltage V_{dc} is considered as a state variable, and the dc-link circuit is shown by Fig. 3.

$$\Delta \dot{V}_{dc} = \frac{\Delta i_b}{C_{dc}} - \frac{\Delta i_r}{C_{dc}}. \tag{12}$$

3.2.4. Grid-side converter

Fig. 3 details the control scheme of the grid-side converter. The converter controller operates in the synchronous rotating grid voltage oriented reference frame, with its d-axis aligned along the grid voltage vector. The linearized model of the grid-side converter is shown by

$$\Delta \dot{i}_{bd} = \frac{-R_b}{L_b}\Delta i_{bd} + \omega_{pll}\Delta i_{bq} + \frac{1}{L_b}\Delta V_{sd} - \frac{1}{L_b}\Delta V_{bd} + I_{bq}\Delta\omega_{pll}\,,\ \Delta\dot{\zeta}_{dc} = -\Delta V_{dc}\,,\ \Delta\dot{\zeta}_{ibd} = \Delta i^{*}_{bd} - \Delta i_{bd}\,,\ \Delta\dot{\zeta}_{pll} = -\Delta V_{sqpll}\,,\ \Delta\dot{\theta} = \Delta\omega_{pll} - \Delta\omega_r. \tag{13}$$

4. Modal analysis-case studies

The state space modelling of the microgrid elements have been detailed. In this section, the stability analysis is established by analyzing the locus of the microgrid critical eigenvalues under different operating conditions. By conducting sensitivity analysis on the system state matrix, the participation of different state variables in a particular mode can be revealed [6]. The sensitivity of the eigenvalue λ_i to the diagonal element a_{jj} of the system state matrix is shown by (14), where p_{ji} is the sensitivity factor.

$$p_{ji} = \frac{\partial \lambda_i}{\partial a_{jj}}. \tag{14}$$

Table 3
Dominant state variables for mechanical torque increment scenario.

λ	Dominant states	Participation factor	Remarks
−0.36+j87	Electrical, δ	0.84	Unstable (Hopf bifurcation)
−0.58	Electrical, v_{dc}	0.68	Unstable (Hopf bifurcation)
−1.93	Mechanical, s	0.32	Unstable (Hopf bifurcation)

4.1. Wind speed impact

Through this scenario, the wind speed is assumed to gradually increase at the ninth bus (B9) from 1.5 m/s to 9 m/s in small time

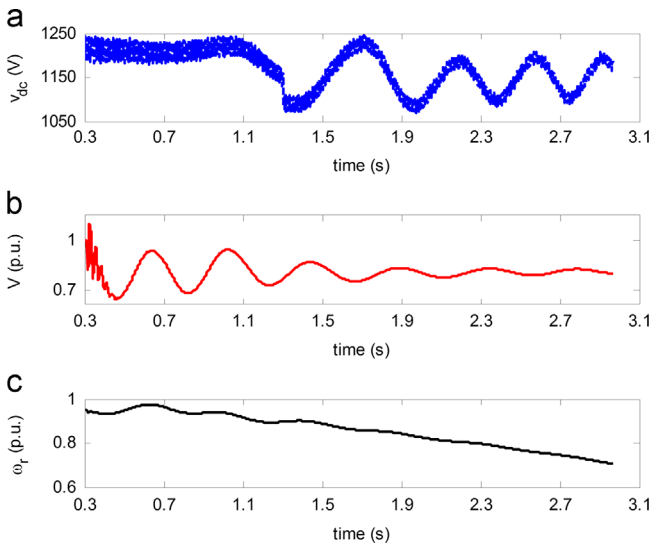

Fig. 11. Effect of mechanical torque increment: (a) dc-link voltage, (b) voltage at B9, and (c) induction motor mechanical speed.

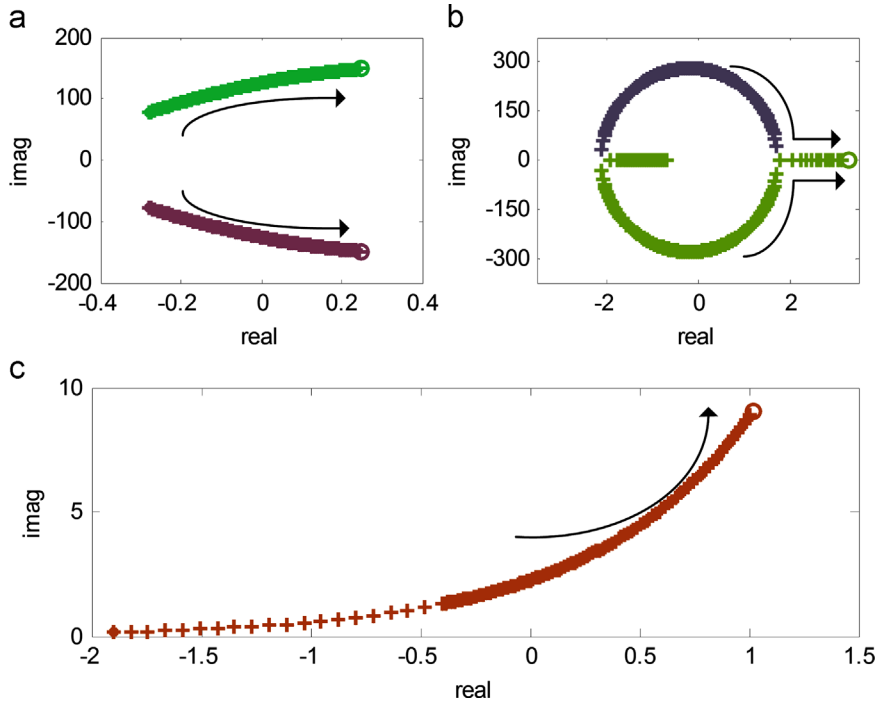

Fig. 10. Eigenvalues loci during mechanical torque increment of modes affected by (a) coordinates' angles of rotation, (b) dc-link voltage, and (c) induction machine slip.

steps, and so the charging level of the batteries is almost constant. Furthermore, the wind speeds at the other microgrid buses are set at a constant value equal to 3 m/s; also the proportional and integral dc-link gains of all DFIGs supplying the microgrid K_{pdc} and K_{idc} are set as 1.1.

Fig. 4 shows that the system is stable through the entire range of wind speeds, but at the same time, it is observed that the critical oscillatory modes mainly affected by the magnetization currents move towards the imaginary axis, raising the possibility of a Hopf bifurcation. Clearly, the dominant modes through current simulation are influenced by either mechanical or electrical state variable of the DFIG at B9. The mechanical state variables include wind turbine speed and the shaft twist angle. On the other hand, the electrical state variables include the DFIG magnetization current. All these modes move towards the imaginary axis with increasing oscillation frequencies. The behaviour of the critical modes associated with the DFIGs state variables with respect to the wind speed increment clarified in this section coincides with the corresponding results shown in [6,10,20]. In [6] the oscillatory modes move towards the imaginary axis, and once the wind speed surpasses the rated speed value of the turbine, the oscillations of the critical modes reduce due to the effect of the pitch control. In this paper, all the simulations are run below the rated speed of the wind turbines, and so the effect of the pitch control can be neglected. In addition, in this paper, the effect of the wind speed increment on the state variables associated with the voltage frequency inverters is investigated.

One of the interesting results in this simulation is that due to the increasing oscillations of DFIG state variables, one other state variable associated with the power controllers of the voltage frequency inverters is stimulated. The growing oscillations of the DFIG state variables cause small perturbations in the voltage nodes across the distribution network. These perturbations accordingly drive the coordinates' angles of rotation to oscillate. Consequently, these state variables start showing oscillatory behaviour and their influenced mode slightly moves towards the imaginary axis. An important conclusion from this scenario is that with wind speed increase, another mode influenced by the DFIG dc-link voltage starts moving towards the imaginary axis with increasing oscillations. Fig. 5 shows the time domain response of dc-link voltage, wind turbine electrical power and node voltage at B9. It is clear that these variables are stable during the simulation. However, slight oscillations of dc-link voltage occur during the final samples of the simulation.

Due to the importance of dc-link voltage for the stability of the DFIG, the control parameters of the dc-link circuits were varied and the effect observed.

Another simulation is processed at different dc-link gain values, as both K_{pdc} and K_{idc} are set as 0.1, in order to clarify the effect of the dc-link state variables on the microgrid stability.

The change that occurs with decrease in the proportional and integral control gains of the dc-link control circuit is that the system became unstable, Fig. 6. The main state variables, which caused the Hopf bifurcations, are the turbine state variables and dc-link voltage. Furthermore, the mode dominated by the coordinates' angles of rotation moves with a sharp slope towards the imaginary axis and with growing oscillations.

Table 1 illustrates the critical modes, they are dominated by the turbine state variables and dc-link voltage. The first column shows the status of the critical eigenvalues at the first simulation sample, while the last column of remarks shows their statuses at the last simulation sample.

Finally, Fig. 7 shows the instability of the microgrid, as the DFIG mechanical speed, dc-link voltage and the node voltage at B9 are no longer constant and show abrupt oscillations.

4.2. Droop coefficient impact

Through the current simulation, the droop gains of the inverter-interfaced generators supplying the isolated microgrid are gradually increased to simulate the reduction of battery units charging levels, and the wind speed in the simulation is 3 m/s.

Table 2 shows the critical modes and their related state variables. The modes dominated by the coordinates' angles of rotation become unstable and cross the imaginary axis by increasing the droops, producing a Hopf bifurcation, Fig. 8(b). The instability caused by voltage frequency inverters affects the voltage profile across the distribution network and subsequently a mode influenced by the dc-link state variables of the DFIGs is stimulated and steps towards the imaginary axis, Fig. 8(d). This result explains that the dynamics of the energy sources, DFIGs and battery units, are coupled. One of the interesting conclusions of this scenario is that the thermostatic load state variable has a significant contribution in one of the dominant modes. Fig. 8 (c) shows the long-term dynamics of the thermostatic load, as one of the modes associated with that state variable approaches the imaginary axis. DFIG magnetization current modes shift towards the imaginary axis, Fig. 8(a). The behaviour of the critical modes associated with the power controller of the voltage frequency inverters state variables (coordinates' angles of rotation) with respect to droop coefficient increment clarified in this section coincides with the oscillatory modes associated with the power controller of the voltage frequency inverters shown in [18,22,23]. In addition, in this paper, the effect of the voltage frequency inverter droop coefficient increment on the state variables associated with the DFIGs and thermostatic loads is investigated.

Fig. 9 illustrates the behaviour of the microgrid during the inverters droop gains increment. Fig. 9 shows that the inverters keep stable till a certain droop gain limit is reached, and the increment above this value motivates synchronization problems.

The thermostatic load is modelled as a multiplicative generic load [24]. The transients of consumed power are represented as

$$P = z_P P_0 \left(\frac{V}{V_0}\right)^{\alpha_t} \tag{15}$$

The load state variable, z_P, has the same effect of the thermostatic load duty cycle. The multiplicative generic model of the thermostatic load is represented by the following differential equation:

$$T_P \dot{z}_P = \left(\frac{V}{V_0}\right)^{\alpha_s} - z_P \left(\frac{V}{V_0}\right)^{\alpha_t} \tag{16}$$

The load time constant, T_P, lasts for several minutes. If the voltage drops, the consumed power will drop as well; however, the load state variables will increase according to (16) causing the consumed power to recover again according to (15). When the voltage changes, the thermostatic load state variable immediately responds to restore the load power and the power starts oscillating, Fig. 9(b). This result coincides with the multiplicative generic load behaviour under voltage disturbances shown in [24]; however, in the current simulation and, due to the long transient dynamics of the load model and the fast dynamics of the inverter, the power cannot be restored and the load power continues endless unbounded oscillations.

Fig. 9 illustrates that the instability case, which results from the droop gains increment, can be classified as subcritical Hopf, due to the unbounded oscillations.

4.3. Power demand impact

In [25], the eigenvalue sensitivity analysis of a composite load model was investigated. The composite load model included a ZIP

and induction motor models. The mechanical torque of the induction machine is constant, which represents the simplest case study for induction machines. Furthermore, the power network includes 10 synchronous generators. In contrast in our case, the power capability of the microgrid is limited.

To the best of our knowledge, the impact of induction machines penetration on isolated microgrids has not been investigated by eigenvalue sensitivity analysis.

The stator, rotor, and mechanical transients characterize the operation of induction machines. Through this analysis, the main focus will be on the mechanical transients, represented by the slip as a state variable, because it is the slowest transient. The differential equation of rotor motion is

$$2H\dot{s} = T_m(s) - T_{e_m}(V,s) \tag{17}$$

The quadratic torque induction machine was modelled as follows:

$$T_m(s) = T_2(1-s)^2 \tag{18}$$

The proposed small signal stability analysis in this section is processed for the microgrid under continuous increment of induction machine mechanical torque at B9, which is supplied by a DFIG. The mechanical torque is gradually increased from 0.9 p.u. to 1.5 p.u.

The instability source of the system originates from three dominant modes, those influenced by the coordinates' angles of rotation, DFIGs dc-link state variables and the induction machine slip. Table 3 illustrates the critical modes and their related state variables.

The finding from this scenario is that the instability is caused by Hopf bifurcations, Fig. 10. The modes associated with the coordinates' angles of rotation and DFIGs dc-link voltage move towards the imaginary axis, crossing to the right unstable side of the s-plane. Fig. 10(c) shows the trajectory of the mode influenced by the induction machine slip, which entails incrementing the mechanical torque. It is clear that incrementing the mechanical torque reduces the stability margin until only one equilibrium point exists. Beyond this equilibrium point, no intersection exists between electrical and mechanical torque, and the stability is subsequently lost. This result is similar to the conclusion shown in [24], where the author investigated the stability margin of the quadratic torque induction machine with respect to different values of the mechanical torque.

Fig. 11 illustrates the consequences of incrementing the mechanical torque. The voltage oscillates and drops after a certain level of mechanical torque increment; subsequently, the dc-link voltage drops and starts unbounded oscillations. Finally, the intersection between the mechanical and electrical torque of the induction motor is lost, and the motor stalls.

5. Conclusion

With the increasing use of energy storage devices and renewable energy sources especially in the rural areas, the inverter-based generators have become vital components in the microgirds. The detailed modelling of isolated microgrids supplied by battery units interfaced via inverters and DFIGs was presented. The interactions of the DFIGs with the inverter-based generators along with the quadratic torque induction machines and thermostatic loads are clarified using small-signal analysis in order to study the network critical modes. Moreover, the similarity between this study's results and other results in the literature were clarified to give credibility to the findings of the paper. The contributions of this paper include: (1) investigation of the stability problems in isolated microgrids and (2) identification of the network critical modes under different disturbances.

For the DFIGs, the critical modes are dominated by the shaft twist angle, turbine angular speed and dc-link voltage state variables. For the battery units interfaced via inverters, the critical modes are dominated by the coordinates' angles of rotation. On the other hand, for the quadratic torque induction motors and thermostatic loads, the critical modes are dominated by the slip and duty cycle state variables, respectively. The experienced bifurcations through different scenarios of sensitivity analyses are related to Hopf bifurcations, which reduce the power capability of the isolated power networks. The time-domain simulations verify the analysis results.

This study would help in establishing robust controllers with preferential treatment to the identified critical modes under different disturbances. An appropriate multi-input multi-output robust control system is currently under development for the proposed microgrid model at Warwick University.

References

[1] Mishra Y, Dong ZY, Ma J, Hill DJ. Induction motor load impact on power system eigenvalue sensitivity analysis. IET Gener, Transm Distrib 2009;3(7):690–700.
[2] Gautom D. Impact of increased penetration of DFIG based wind turbine generators on rotor angle stability of power system. Phoenix, AZ, USA: Department of Electrical Engineering, Arizona State University; 2010 [PhD thesis].
[3] Atwa YM, El-saadany EF. Probabilistic approach for optimal allocation of wind-based distributed generation in distribution systems. IET Renew Power Gener 2011;5(1):79–88.
[4] Lasseter RH, Eto JH, Schenkman B. CERTS microgrid laboratory test bed. IEEE Trans Power Deliv 2011;26:325–32.
[5] Kroposki B, Lasseter R, Ise T, Morozumi S, Papatlianassiou S, Hatziargyriou N. Making microgrids work. IEEE Power Energy Mag 2008;6(3):40–53.
[6] Yang L, Zhao Xu. Oscillatory stability and eigenvalue sensitivity analysis of a DFIG wind turbine system. IEEE Trans Energy Convers 2011;26:328–39.
[7] Yang L, Yang GY, Xu Z. Optimal controller design of a doubly-fed induction generator wind turbine system for small signal stability enhancement. IET Gener, Transm Distrib 2010;4:579–97.
[8] Miao Zhixin, Fan Lingling, Osborn D, Yuvarajan S. Control of DFIG-based wind generation to improve interarea oscillation damping. IEEE Trans Energy Convers 2009;24(2):415–22.
[9] Ostadi A, Yazdani A, Varma RK. Modeling and stability analysis of a DFIG-based wind-power generator interfaced with a series-compensated line. IEEE Trans Power Deliv 2009;24(3):1504–14.
[10] Mishra Y, Mishra S, Fangxing Li, Yang Dong Zhao, Bansal RC. Small-signal stability analysis of a DFIG-based wind power system under different modes of operation. IEEE Trans Energy Convers 2009;24(4):972–82.
[11] Mishra Y, Mishra S, Fangxing Li. Coordinated tuning of DFIG-based wind turbines and batteries using bacteria foraging technique for maintaining constant grid power output. IEEE Syst J 2012;6(1):16–26.
[12] Miao Zhixin, Domijan A, Fan Lingling. Investigation of microgrids with both inverter interfaced and direct AC-connected distributed energy resources. IEEE Trans Power Deliv 2011;26(3):1634–42.
[13] Bottrell N, Prodanovic M, Green TC. Dynamic stability of a microgrid with an active load. IEEE Trans Power Electron 2013;28(11):5107–19.
[14] Hassan MA, Abido MA. Optimal design of microgrids in autonomous and grid-connected modes using particle swarm optimization. IEEE Trans Power Electron 2011;26(3):755–69.
[15] Wang Chengshan, Li Yan, Peng Ke, Hong Bowen, Wu Zhen, Sun Chongbo. Coordinated optimal design of inverter controllers in a micro-grid with multiple distributed generation units. IEEE Trans Power Syst 2013;28(3):2679–87.
[16] Kuh ES, Rohrer RA. The state-variable approach to network analysis. In: Proceedings of the IEEE; 1965. p. 672–86.
[17] Chen SX, Gooi HB, Wang MQ. Sizing of energy storage for microgrids. IEEE Trans Smart Grid 2012;3(1):142–51.
[18] Pogaku N, Prodanovic M, Green TC. Modeling, analysis and testing of autonomous operation of an inverter-based microgrid. IEEE Trans Power Electron 2007;22(2):613–25.
[19] Diaz G, Gonzalez-Moran C, Viescas C. State-space representation of DFIG-based wind power plants. IET Renew Power Gener 2013;7(3):254–64.
[20] Mei F, Pal BC. Modal analysis of grid-connected doubly fed induction generators. IEEE Trans Energy Convers 2007;22:728–36.
[21] Hinrichsen EN, Nolan PJ. Dynamics and stability of wind turbine generators. IEEE Trans Power Appl Syst 1982;101(8):2640–8.
[22] Mohamed Y, El-Saadany EF. Adaptive decentralized droop controller to preserve power sharing stability of paralleled inverters in distributed generation microgrids. IEEE Trans Power Electron 2008;23:2806–16.
[23] Barklund E, Pogaku N, Prodanovic M. Energy management in autonomous microgrid using stability-constrained droop control of inverters. IEEE Trans Power Electron 2008;23:2346–52.
[24] Thierry V, Costas V. Voltage stability of electric power systems. Springer; 1998.

[25] Mishra Y, Dong ZY, Ma J, Hill DJ. Induction motor load impact on power system eigenvalue sensitivity analysis. IET Gener, Transm Distrib 2009;3 (7):690–700.

Ahmed M. Abd el Motaleb received the B.S. degree in electrical engineering from Ain Shams University, Cairo, Egypt in 2005, and M.S. degree from Sevilla University, Spain in 2010. Finally, he received the Ph.D. degree in electrical and electronic engineering from University of Oviedo, Spain, 2013. He is currently a research fellow at University of Warwick, UK.

His areas of interest include microgrid analysis, distributed energy sources, and system control and coordination with HVDC.

Dean P. Hamilton, after completing his first degree and Master's degree in Systems Engineering at the University of York, joined the system's design team at Marconi Communications where he worked on advanced high speed data switching systems, and eventually became a member of Ericsson's next generation developments team. He later obtained his PhD at the University of Warwick and has since been a researcher in the power electronics team at the School of Engineering. He worked as part of a team to develop a back-to-back inverter test rig for Toyota, Japan, to emulate the conditions seen by the IGBTs in their Prius inverter, and then on an electric vehicle project to evaluate SiC MOSFETs and packaging. His current project and interests are in SiC inverters and control, device reliability and high temperature power module packaging for use in future electric vehicle powertrains and renewable energy systems.